Evaluation of Soil Moisture Effects on the Generation and Modification of Mesoscale Circulations

Y. OOKOUCHI[1], M. SEGAL, R. C. KESSLER AND R. A. PIELKE

Department of Atmospheric Science, Colorado State University, Fort Collins, CO 80523

(Manuscript received 26 January 1984, in final form 20 August 1984)

ABSTRACT

The current study provides an evaluation of thermally induced circulation over flat terrain due to nonuniform horizontal distribution of soil moisture availability. Additionally, the effect of soil moisture availability on the thermally induced upslope flow during the daylight hours is examined. The results indicate that in flat terrain, which has a nonhomogeneous moisture availability, the intensity of thermal circulations approaches that of sea-breeze circulations for the case of large contrasts. Even small amounts of water in the soil, adjacent to dry areas, can still result in a significant mesoscale flow. The upslope flow has been indicated to be perturbed significantly when the moisture availability increases or when the horizontal contrast of soil moisture availability becomes large.

1. Introduction

Thermally induced mesoscale circulations that are associated with terrain inhomogeneities (e.g., those involved with sea–land, urban–rural areas and mountainous regions), have been widely studied using both observational and modeling methodologies. These calculations frequently have seasonal persistence with a significant diurnal cycle and therefore are easily detectable in routine data.

The surface sensible heat flux is a prime forcing mechanism of the planetary boundary layer (PBL) thermal characteristics. Therefore, the partition of energy between the sensible and the latent heat fluxes at the surface (i.e., the Bowen ratio) is a key factor in the development of the PBL. The Bowen ratio depends on the amount of ground moisture; its value ranges from infinity in arid regions to less than one over very wet soils.

Soil moisture has been indicated by observational studies and by one-dimensional modeling studies (e.g., Philip, 1957; Sasamori, 1970; Zdunkowski *et al.*, 1975; Deardorff, 1978; Carlson and Boland, 1978; Wetzel, 1978; and Zhang and Anthes, 1982), to have a major effect on the characteristics of the surface heat budget, and, therefore, on the characteristics of the PBL. Zhang and Anthes (1982), for example, have concluded that the variations of the soil moisture within normal ranges, have more significant effects on PBL characteristics than frequently observed changes of surface albedo, surface roughness or soil thermal capacity.

Several factors may contribute to the variability of soil moisture within a mesoscale domain:

- The sporadic distribution of convective precipitation can create, temporarily, isolated areas with high amounts of soil moisture.
- Topographic influences can result in seasonal spatial differences in precipitation between the windward and the lee sides of mountain ranges, as well as cause changes of precipitation with elevation. Consequently, seasonal differences in soil moisture in such cases are expected.
- Agricultural irrigation (mostly in semiarid regions), might produce sharp contrasts in the soil moisture between the cultivated area and its surroundings.
- Regions that include marsh areas may also be associated with variability in the surface moisture.

Considering the results of the aforementioned studies, which evaluated the effect of soil moisture on the surface thermal balances and the PBL characteristics, it is expected that horizontal discontinuities in the soil moisture induce significant discontinuities in surface thermal forcing and, consequently, mesoscale circulations. Such circulations, which are associated with terrain inhomogeneities, may play an important role in patterns relating to local meteorology, cumulus convection and air quality.

Studies by Lanicci and Carlson (1983), Benjamin (1983) and Carlson *et al.* (1983) evaluated the effect of soil moisture contrasts on the synoptic scale. Sun

[1] Present affiliation: Yatsushiro National College of Technology, Yatsushiro, 866, Japan.

and Ogura (1979) used a mesoscale model to study the possible induced circulations along drylines in the Great Plains for a specific case study in which the effects of surface conditions on the PBL were prescribed.

The effect of soil moisture on terrain-induced mesoscale circulations is also expected to be significant. McCumber (1980) and Physick (1980), for example, have found that sea-breeze intensity decreases as soil moisture increases. Also, based on the sea-breeze studies, it is likely that soil moisture exerts a major effect on topographically induced thermal flows.

Manabe (1969) defines the soil moisture availability such that

$$m = \frac{E}{E_p}, \tag{1}$$

where E is the surface evaporation rate and E_p is the potential evaporation rate at the surface. The value of m can range from zero to 1, providing a measure of the soil wetness.

Carlson *et al.* (1981), for example, inferred the distribution of soil moisture in two urbanized areas by analyzing infrared satellite temperature measurements in conjunction with a one-dimensional PBL model. They indicated values of m which are >0.7 for completed vegetated areas, 0.4 for suburban sites, and <0.3 for the industrial and commercial district in the Los Angeles area, where 1.0 corresponds to a water surface.

We will refer to a spatial discontinuity in soil wetness as a soil moisture contrast. The object of this study is to evaluate the intensity of mesoscale circulations that are induced by mesoscale soil moisture contrasts, and the modification of these circulations in the presence of topography. Numerical model evaluations were considered for the following situations:

i) soil moisture contrasts along flat terrain,
ii) soil moisture contrasts along mountain slopes.

Additionally, we examined the effect of different values of soil moisture, distributed homogeneously along mountain slopes, on thermally induced upslope flows.

In the absence of observational evaluations of such situations, the intention of this study is mainly to provide a rough estimate of the relative effect of soil moisture discontinuities on mesoscale flows. Existing validation studies with the model (see Section 2) provide some confidence in the accuracy of the current simulations. Modeling aspects pertinent to the current study are given in Section 2. The results are described in Section 3 (focusing mainly on the daylight hours because during this period of the day evaporation from the surface is generally much more significant than at night).

2. The model and initial conditions

The formulation of the numerical model utilized in the current study is given in detail by Pielke (1974), Mahrer and Pielke (1977a) and McNider and Pielke (1981). Validation studies with that model have indicated reasonable skill in the resolution of mesoscale airflow patterns (e.g., Pielke and Mahrer, 1978; Segal and Pielke, 1981; and Segal *et al.*, 1982). McCumber and Pielke (1981) introduced into the model a detailed one-dimensional parameterized formulation for soil physics. However, since in the current study we desire only a rough estimate of the sensitivity of the simulated airflows to soil moisture contrasts, a simplified routine for the soil formulation is used. It consists of solving the equation of thermal conduction in soil:

$$\rho_s C_s \frac{\partial T}{\partial t} = \lambda \frac{\partial^2 T}{\partial z^2}$$

with

$$\lambda = \rho_s C_s \kappa_s, \tag{2}$$

where T is the soil temperature, ρ_s soil density, C_s soil heat capacity, λ heat conductivity and κ_s soil heat diffusivity coefficient.

The soil moisture content is assumed to be homogeneous with depth, and its contribution to the surface value of the specific humidity q_G is given according to

$$q_G = q(z_1)(1 - m) + m q_s(T_s), \tag{3}$$

where $q_s(T_s)$ is the saturated specific humidity at the temperature of the soil surface T_s; $q(z_1)$ is the specific humidity at the first level of the model, and m is the measure of the soil wetness as defined in the previous section. The aerodynamic roughness for these experiments is assumed to be 4 cm.

The temperature at the soil–air interface is calculated using a thermal balance equation which includes solar radiation, incoming longwave radiation, latent, sensible and soil heat fluxes and the outgoing surface longwave radiation. Parameterizations of the effects of soil moisture on the albedo, soil heat capacity and diffusivity are included. In these computations the soil wetness was approximated as linearly related to m [with $m = 0$ (dry soil) and $m = 1$ (saturated soil)]. The dependence of soil heat capacity and diffusivity on soil moisture and temperature is calculated according to De Vries (1963). Figure 1 illustrates the relations among the soil moisture availability m, the thermal diffusivity κ_s, the heat capacity $\rho_s C_s$ and the soil thermal conductivity λ. The relations are presented for a soil temperature of 25°C; however, only small changes in those variables are caused as soil temperature changes. To evaluate the effect of soil moisture on albedo, we adopted the following relation, based on Idso *et al.* (1975) and Deardorff (1978):

$$A = 0.31 - 0.17\ \mathrm{m}. \tag{4}$$

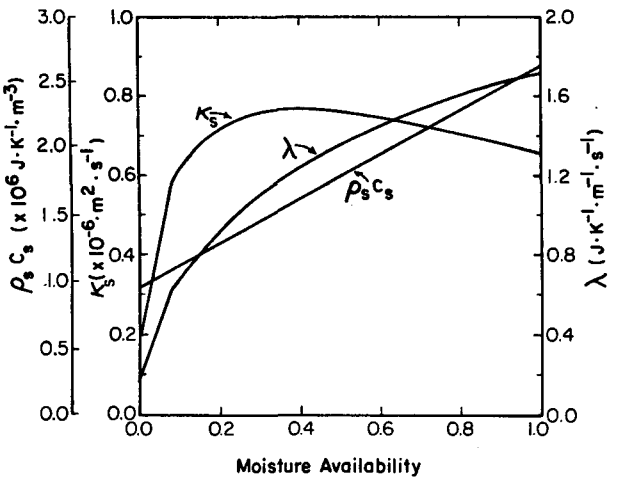

FIG. 1. The relation between soil moisture availability m and several physical properties of the soil: κ_s, soil heat diffusivity coefficient; λ, soil heat conductivity; $\rho_s C_s$, soil heat capacity for a unit volume (based on De Vries, 1963).

The model in the current study (two-dimensional version) consists of 14 vertical levels (5, 15, 50, 100, 300, 500, 700, 900, 1200, 1500, 2000, 3000, 5000 and 7000 m) with a top at 7000 m. The model horizontal grid interval is 5 km and the time step used in the simulation is 90 s. The beginning of the simulation is 0800 LST, while summer day conditions, adapted from a previous simulation (Segal *et al.*, 1983) in central Israel (latitude 32°), were used for the model initialization. In the current study, only a very slight (northerly) synoptic flow (0.5 m s^{-1}) is assumed. The initial conditions for specific humidity and temperature consist of a moderately moist lower atmosphere capped with a slight upper layer inversion as given in Fig. 2.

3. Simulation results

The simulations conducted in our study are summarized in Table 1, which will be followed by the discussion of the results. In the vertical cross section illustrations (Fig. 3), the dark line indicates the wet soil portion of the domain.

a. Flat terrain simulations

Five degrees of soil wetness contrasts, ranging from a relatively mild soil moisture contrast (F1) to an extremely sharp contrast (F5) were simulated. In order to evaluate the possible effects of a relatively sharp soil moisture contrast, the results of simulation F4 are discussed in detail. Figs. 3a, b present vertical cross sections of the U and V components at 1600 LST. A pronounced circulation is predicted at this hour, with a noticeable return flow. The veering of the induced flow due to the Coriolis effect is reflected through the V component. Following sunset (at 2000 LST), an intensification of the circulation and its eastward progress is evident (Figs. 3c, d). Similar behavior in observed and modeled sea-breeze patterns following sunset has been observed by Simpson *et al.* (1977).

In the situation of weak synoptic flow, the turbulence in the lower atmosphere becomes negligible at night because of the stabilization of the PBL. The following patterns appear by midnight (Figs. 3e, f):

i) Additional eastward penetration of the circulation. Clarke (1983) notes a similar behavior of the sea breeze during the nocturnal hours along the coast of Australia. This penetration apparently occurs because the flow above the surface layer becomes decoupled from the nocturnal boundary layer.

ii) Rotation of the U component of the wind produced during the day to a V component due to the Coriolis force.

When this conversion to a predominantly V-component flow occurs, the eastward propagation of the circulation is terminated.

With a milder contrast of soil moisture availability, similar patterns to those described above were obtained. However, as expected, the intensities of the circulations were reduced, while the F5 results were similar to that of a sea-breeze (SB) case. Figure 4, in which the maximum wind speeds at 5 m height for various cases are plotted as a function of time, provides some idea of the effect of the soil moisture contrasts on the intensity of the mesoscale flow. Comparison of the maximum wind speeds obtained in simulation F5 with those obtained in a sea-breeze

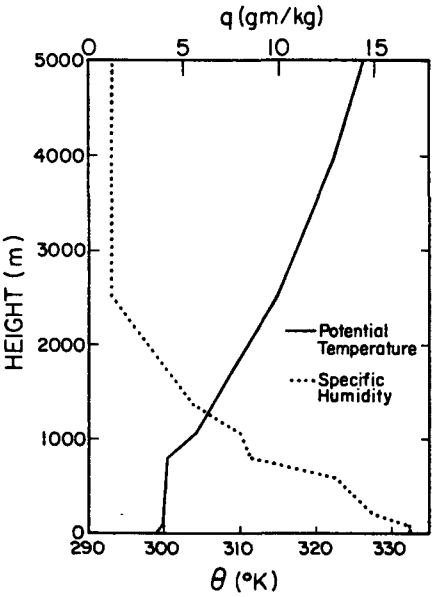

FIG. 2. The initial conditions for potential temperature and specific humidity.

TABLE 1. Summary of the simulated cases (based on soil moisture characteristics and the simulated domain topography).

Case	Soil moisture availability (m)		Slope angle	Topography
	Western section	Eastern section	(tan α)	
SB	(sea)	0.05	0	flat terrain
F1	0.1	0.05	0	flat terrain
F2	0.2	0.05	0	flat terrain
F3	0.3	0.05	0	flat terrain
F4	0.5	0.05	0	flat terrain
F5	1.0	0.05	0	flat terrain
M1	0.05	0.05	2/100	symmetric mountain†
M2	0.5	0.5	2/100	symmetric mountain†
M3	0.5	0.05	2/100	symmetric mountain†
S1	0.05	0.05	2/100	single slope
S2	0.5	0.5	2/100	single slope
S3	0.5	0.05	2/100	single slope
S4	0.05	0.5	2/100	single slope
S4*	0.05	0.5	1/100	single slope

† Top of mountain is 800 m.

simulation (case SB, in which the area of wet soil was replaced by a body of water whose surface temperature is held equal to the initial temperature of the land surface), indicates that a boundary between saturated and dry soils can induce a circulation whose intensity is close to that of a sea breeze. The results suggest, also, that even a mild contrast in soil moisture availability m (0.05–0.1) may exert a measurable effect on the airflow. Such a conclusion was also implied indirectly by Mahrer and Pielke (1978).

Figure 5 provides an estimate of the circulation intensity using the maximum predicted vertical velocities in the computation domain as a function of time. The first peak values occur in the early afternoon hours, while a second peak occurs in the early evening. The second peak is associated with the intensification of the horizontal gradient of the U component as a nocturnal jet is established.

The soil surface temperature differences ($\Delta\bar{T}$) between the wet and the dry domains, as averaged for 50 km on each side of the contrast line, are illustrated in Fig. 6. They provide an indirect indication of the expected circulation intensities. During the nocturnal period this temperature difference becomes relatively small as evaporation from the soil is reduced. However, $\Delta\bar{T}$ increases sharply as Δm increases from 0.05 (F1), to 0.45 (F4), across the contrast line; the rate at which $\Delta\bar{T}$ increases is reduced as Δm approaches 0.95 (F5). This reduced rate of change when Δm is large is also reflected in the rate of change of the horizontal wind speed and vertical velocity, which are shown in previous figures.

Figure 7 presents $\Delta\bar{T}_{\max}$ and $U_{\max}$ as a function of the soil moisture contrasts for the various simulated cases. In these relations, $\Delta\bar{T}_{\max}$ is the daily maximum value of $\Delta\bar{T}$ for each case (which occurs around 1200–1400 LST), and $U_{\max}$ is the daytime maximum value for the surface U component (which occurs around 1600–1800 LST). The log linear equations shown in this figure provide excellent representations of the simulated values of $U_{\max}$ and $\Delta\bar{T}_{\max}$ as Δm ranges from 0.15 to 0.95. These equations suggest the following relation between $U_{\max}$ and $\Delta\bar{T}_{\max}$:

$$U_{\max} = 0.20\Delta\bar{T}_{\max} + 1.9 \text{ (m s}^{-1}\text{)}. \quad (5)$$

It is worth noting that, based on similarity considerations, Biggs and Graves (1962), and Lyons (1972) suggested a criterion for a sea-breeze occurrence when an offshore synoptic flow V_g exists. The sea breeze is developed if

$$V_g^2 < \beta\Delta\bar{T}_{LS}, \quad (6)$$

where β is an empirical constant and $\Delta\bar{T}_{LS}$ is the maximum land sea temperature difference observed during the day. According to Walsh (1974), $\beta = 1.5$. If a simple linear composition is assumed for resultant opposing winds, this criterion provides the typical intensity of the sea breeze V_{SB} in the absence of any synoptic flow, namely,

$$V_{SB}^2 \approx \beta\Delta\bar{T}_{LS}. \quad (7)$$

We approximated the induced flow in our cases based on (7). The open circles in Fig. 7 indicate values for V_{SB} obtained by using (7). They indicate agreement with the simulated values, which suggests that (7) is a reasonable formulation with which to estimate the flow intensity due to a soil moisture contrast.

b. *Mountain cases*

Soil moistening is also expected to modify thermal circulations along mountain slopes. The influence on

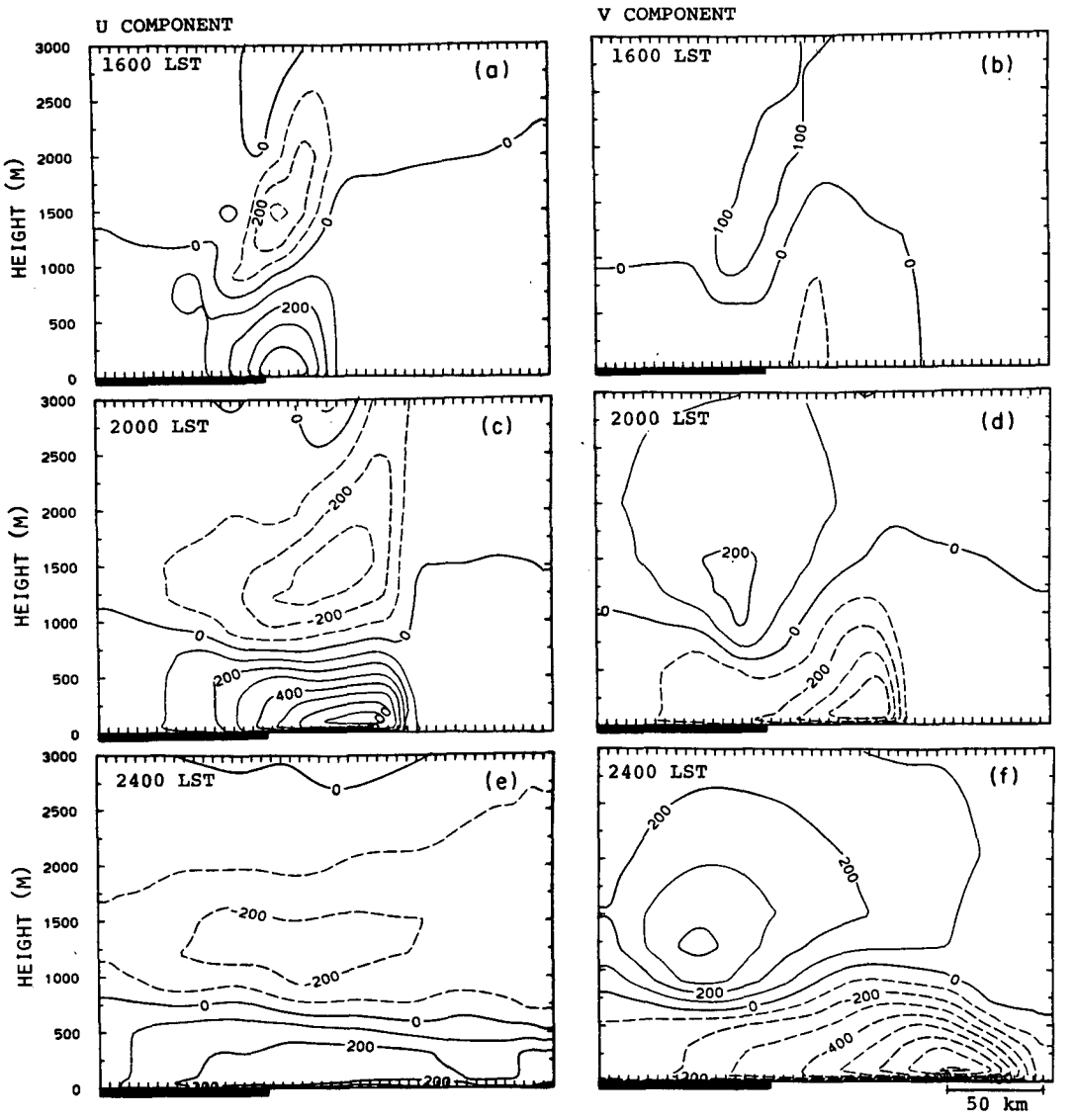

FIG. 3. West–east vertical cross section of the simulated domain presenting the U (west–east) and V (south–north) components (cm s^{-1}) for case F4 for several selected hours (dashed contours indicate negative component—easterly). The heavy line indicates the wet portion of the domain (m = 0.5) which is adjacent to a dry soil (m = 0.05).

these thermal circulations are expected to be complex when the soil moisture availability is spatially non-uniform. We have investigated the magnitude of these effects for two cases: i) a symmetric mountain case and ii) a single slope case.

1) SYMMETRIC MOUNTAIN

The major role that soil moisture plays in the development of the daytime upslope circulation is illustrated in Fig. 8. The reduction of sensible heat fluxes along the wet slopes in case (M2) results in a considerably weaker upslope circulation than obtained in case (M1).

As stated in Section 1, mountains sometimes have a relatively wet slope on one side, contrasted by a relatively dry slope on the opposite side. The development of a daytime upslope circulation in such a case (M3) is presented at the bottom of Fig. 8. These results suggest that, in addition to the development of upslope winds on each side of the mountain, an overflow from the wet side toward the dry slope occurs. The overflow is induced by a net pressure gradient between both sides, resulting from the overall difference of thermal heating along the slopes. The airflow in case M3 resembles, to a certain extent, the airflow induced by the presence of a sea adjacent to a mountain, such as obtained by Mahrer and Pielke

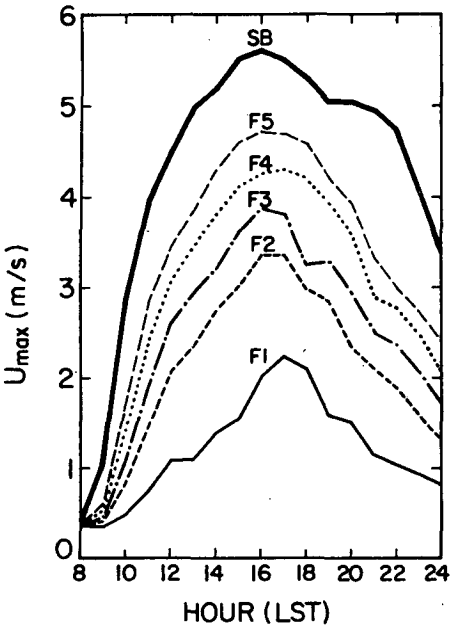

FIG. 4. The maximum wind speed (m s^{-1}) at 5 m height along the domain cross section, for various soil availability contrasts, as a function of time. Flat terrain cases.

(1977b) and Ookouchi *et al.* (1978) on the inland side of the mountain in the afternoon.

Analysis of the terms in the circulation tendency equation for case M3 can provide additional insight into the role of the various components in the determination of the final flow pattern. Following

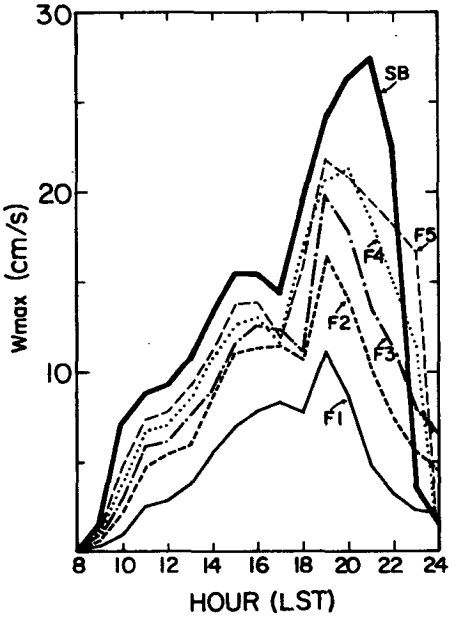

FIG. 5. The maximum vertical wind speed (cm s^{-1}) in the simulated domain cross section, for various soil availability contrasts, as a function of time. Flat terrain cases.

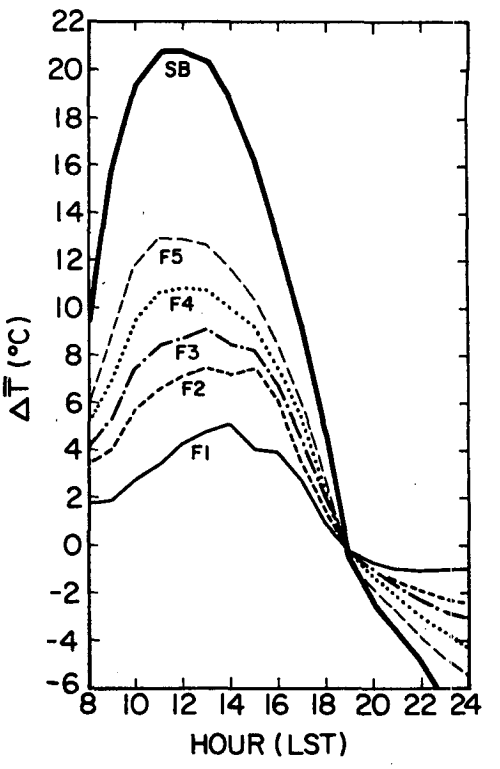

FIG. 6. The surface temperature contrast $\Delta\bar{T}$ between dry and wet domains, for various moisture availability contrasts, as a function of time.

McNider and Pielke (1981) and Segal *et al.* (1983), the circulation tendency $\partial C/\partial t$ along the path of integration as indicated in Fig. 9, assuming frictionless flow, is given by

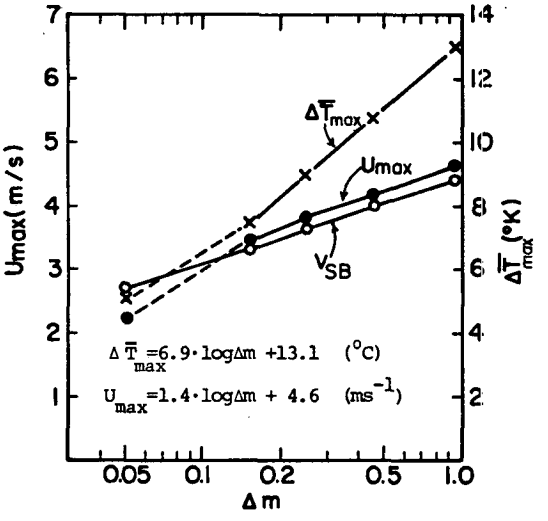

FIG. 7. Log-linear dependence of U_{max} (the maximum U at the surface along the domain cross section) and $\Delta\bar{T}_{max}$ as a function of the difference in the soil moisture availability Δm ($\Delta m = m - m_0$, where $m_0 = 0.05$). The open circles indicate wind speed values obtained from Eq. (7).

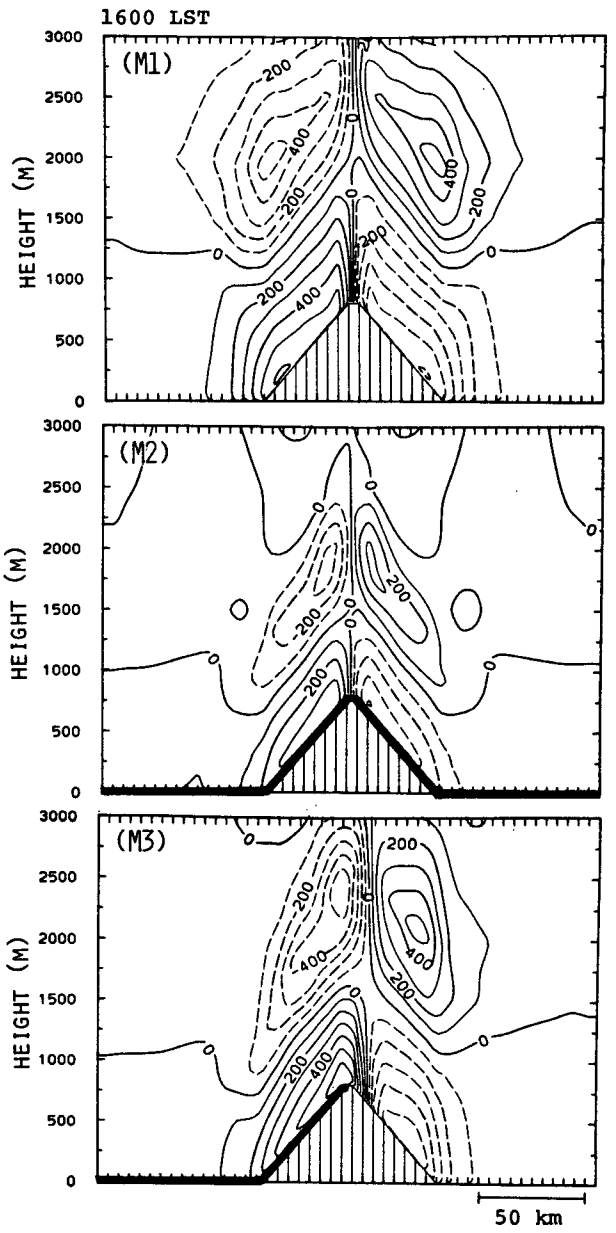

FIG. 8. Vertical cross section of the simulated domain presenting the U (west–east) component (cm s^{-1}) for cases M1, M2 and M3 at 1600 LST (dashed contours indicate a negative component—easterly). The heavy line indicates the wet portion of the domain.

$$\frac{\partial C}{\partial t} = \frac{\partial}{\partial t}\oint \mathbf{u}d\mathbf{l} \approx \int_S \left(-\frac{\partial \theta'}{\partial z^*}\times\frac{\partial z_G}{\partial x} + \frac{\partial \theta'}{\partial x}\right)\left(-\frac{\partial \bar{\pi}}{\partial z^*}\right)dS, \quad (8)$$

where z^* is the vertical coordinate (in a terrain-following coordinate system), $\partial z_G/\partial x$ the terrain slope, π the Exner function for pressure, θ potential temperature, S the area enclosed within the path, an overbar indicates an initial equilibrium state value and a prime a deviation from the initial value. The right-hand integral is applied to the area within the path of integration. The top of the chosen path coincides with the top of the PBL where no contributions to the circulation are expected. This segment roughly divides the opposing flows of the circulation so that the velocity along it is negligible; see, e.g., Anthes, 1978; Mizzi and Pielke, 1984. Contributions from vertical segments are also negligible because w is small relative to u. Hence, in this case,

$$\frac{\partial C}{\partial t} = \frac{\partial}{\partial t}\int_A^B u_s dl, \quad (9)$$

where u_s is the wind speed near the surface, and the line section A–B is the typical horizontal section in which the circulation is noticeable.

Since development of a nearly adiabatic PBL occurs even in the region with highly moistened soil, we assume

$$\frac{\partial(\bar{\theta} + \theta')}{\partial z^*} \approx 0, \quad (10)$$

implying

$$\frac{\partial \theta'}{\partial z^*} \approx -\frac{\partial \bar{\theta}}{\partial z^*}. \quad (11)$$

Using (11) in the evaluation of (8) and substituting $\partial\bar{\pi}/\partial z^* \approx -g/\bar{\theta}$,

$$\frac{\partial}{\partial t}\oint u_s dl \approx \int_{S_0} \frac{\partial \bar{\theta}}{\partial z^*}\frac{\partial z_G}{\partial x}\frac{g}{\bar{\theta}}dS + \int_S \frac{\partial \theta'}{\partial x}\frac{g}{\bar{\theta}}dS$$

$$\approx \int_{S_0} \frac{\partial \bar{\theta}}{\partial z^*}\frac{\partial z_G}{\partial x}\frac{g}{\bar{\theta}}dS + HL\frac{(\theta'_2 - \theta'_1)}{L}\times\frac{g}{\bar{\theta}}, \quad (12)$$

where $H = (H_1 + H_2)/2$ and L is the horizontal extent of the mountain slope. [Note that the two terms on the right-hand side of (12) oppose each other.]

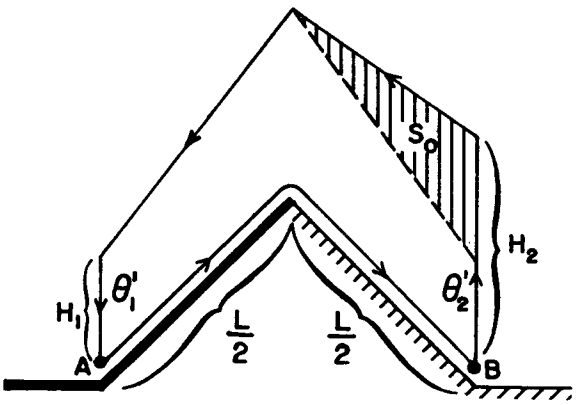

FIG. 9. Schematic illustration of the chosen path of integration for the circulation evaluation for case M3. The top path reflects the PBL top.

The right-hand integral in (12) reflects the buoyancy imbalance between the wet and dry slopes. A similar analysis for flat terrain with the same soil moisture contrast, assuming the same PBL characteristics, yields

$$\frac{\partial}{\partial t}\int_A^B u_s dl \approx H\frac{g}{\bar{\theta}}(\theta'_2 - \theta'_1). \qquad (13)$$

Comparing the relations (12) and (13) implies that the average surface u_s component of the wind along the cross section in M3 should be smaller than the corresponding one in the flat terrain case (F4) (assuming that a larger circulation tendency reflects a buildup of larger wind speeds). Figure 10 presents the wind speed near the surface as a function of time and location for cases (F4) and (M3). The magnitude of surface circulation, indicated on the right of the figure, shows that at 1600 LST in the mountain case, the overall circulation ($\int_A^B u_s dl$) is about half of that corresponding to the flat terrain.

If we assume that changes of the slope angle will have no major effect on the thermal properties of the PBL, then the second term on right-hand side of (12) will not be changed. On the other hand, steepening of the slope will increase the magnitude of the first term on the right-hand side of (12). Since the terms oppose each other, the overall circulation intensity decreases with the steepening of the slope (and, therefore, the flow along both slopes will tend to become more symmetric).

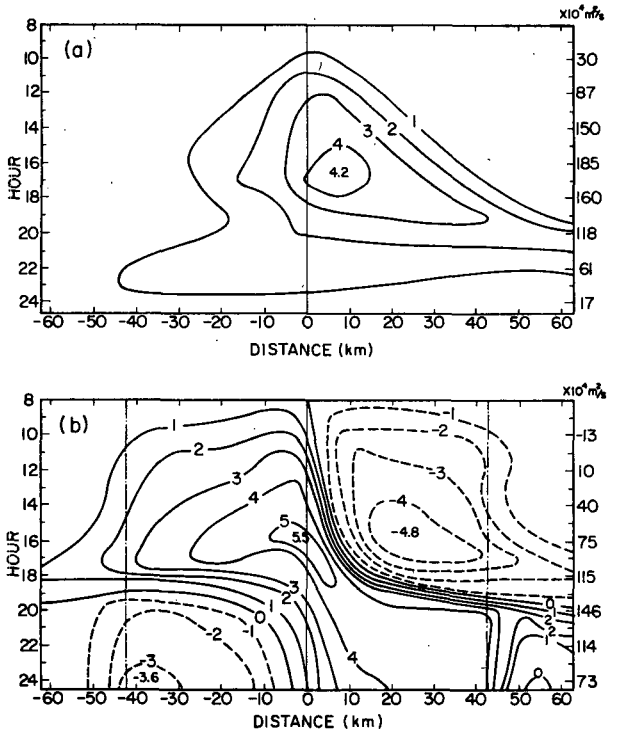

FIG. 10. The surface u_s component (m s^{-1}) at a height of 5 m as dependent on location and time for (a) case F4 and (b) case M3. The surface circulation $\int_A^B u_s dl$ for each hour is given on the right side of each figure.

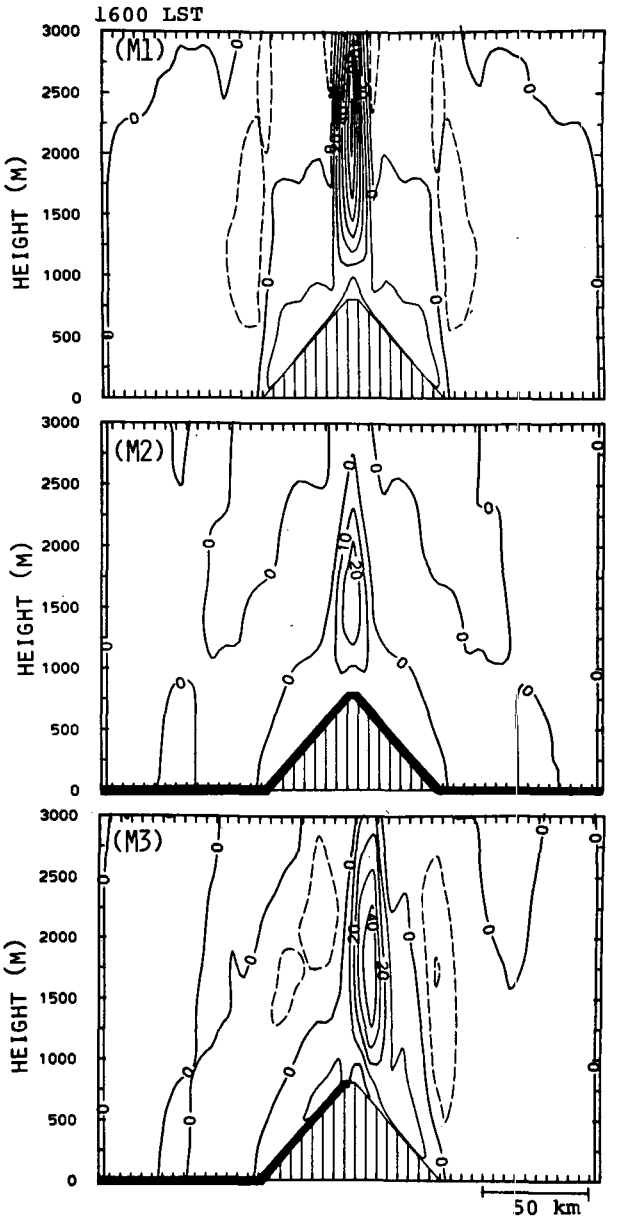

FIG. 11. Vertical cross section of the simulated domain presenting the vertical velocity (cm s^{-1}) for cases M1, M2 and M3 at 1600 LST (dashed contours indicate negative velocity).

The effect of the soil moisture on the convergence of the opposing upslope flows can be evaluated from Fig. 11. The vertical velocity peak, as resolved by the current horizontal grid, was over 70 cm s^{-1} at the mountain top in case M1, while it was reduced significantly (to 30 cm s^{-1}) when the slope had a high moisture availability. Intermediate peak values are predicted for the asymmetric case (M3).

Thermally induced upslope circulations, if they

contain sufficient moisture, are able to enhance development of late afternoon convective clouds. Hence, it is of interest to examine the upward penetration of moisture in these three cases. Figure 12 suggests that for M2, considerable moisture is available, although its upward advection is weak. The sharp vertical gradient of the specific humidity indicates the top of the PBL. The top of the PBL in this case is relatively low because of the evaporative cooling of the surface. Therefore, upward transfer of moisture by turbulence is also limited to this shallow layer. In the dry case (M1), the upward penetration of moisture is deeper

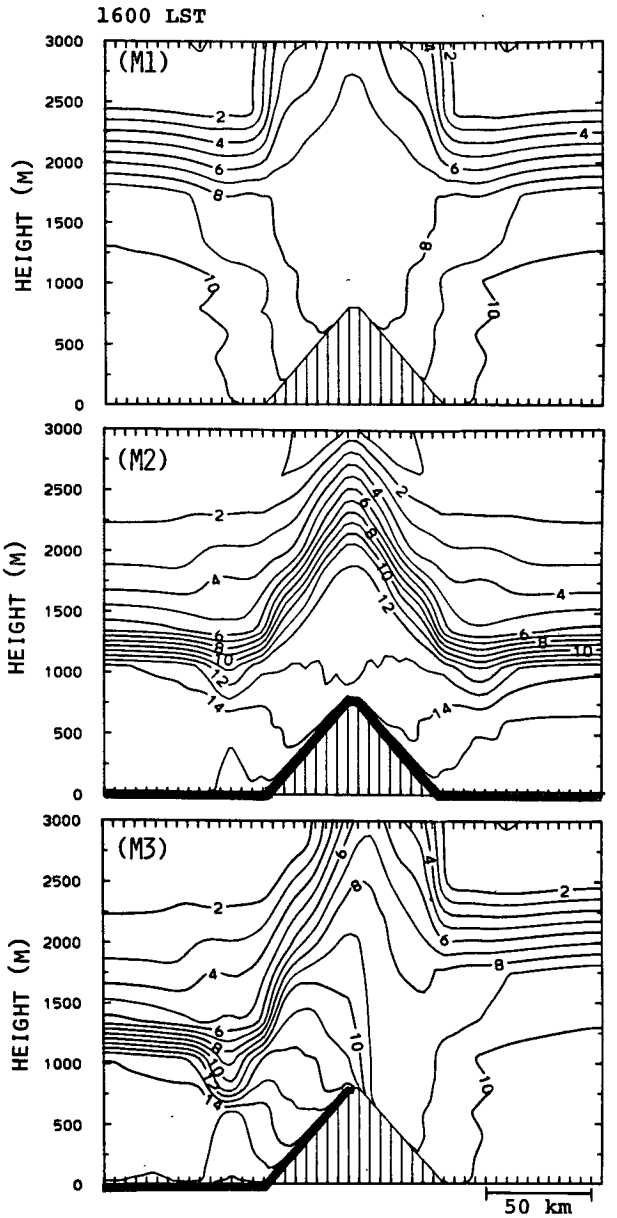

FIG. 12. Vertical cross section of the simulated domain presenting the specific humidity (g kg^{-1}): cases M1, M2 and M3.

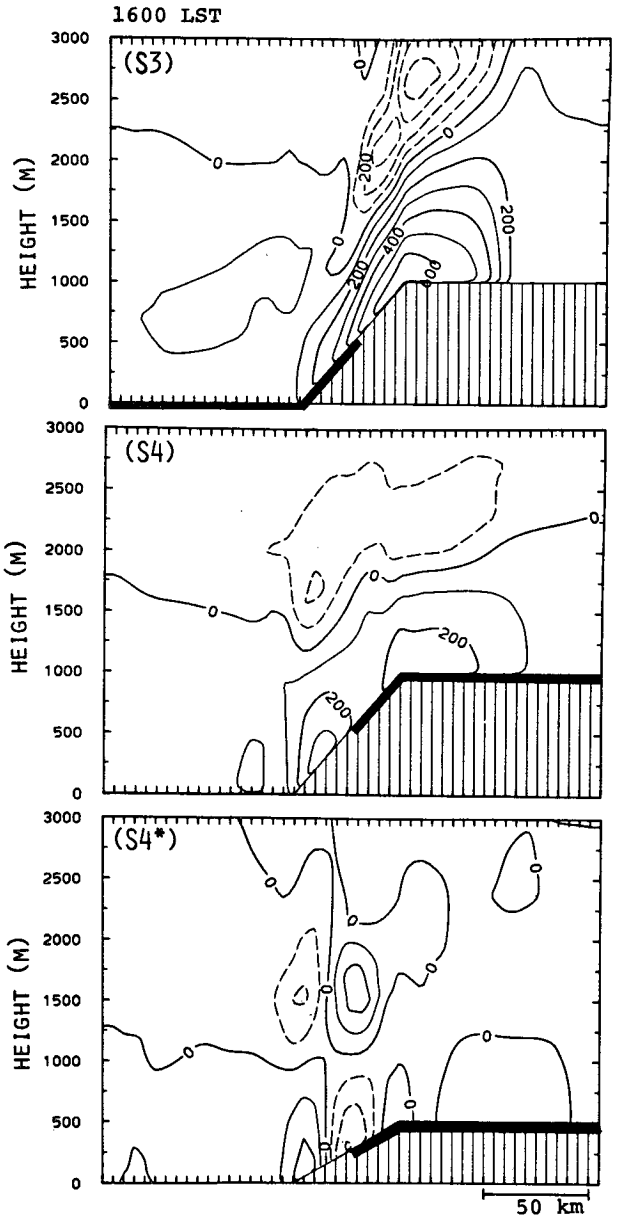

FIG. 13. As in Fig. 8 except for the single slope case: cases S3, S4 and S4*.

than in M2. In such situations, the supply of external moisture to the atmosphere due to synoptic advection may provide an opportunity for a deep upward penetration of additional moisture. In the case of M3, upward penetration of moisture is predicted to be similar to that in case M1.

2) SINGLE SLOPE CASE

In this subsection, the effect of nonhomogeneous soil moisture along a slope which is adjacent to a plateau is evaluated. Frequently, elevated slopes of a mountain receive more precipitation than lower re-

gions. This situation is reflected in cases S4 and S4*. On the other hand, in semiarid regions, agricultural activities along the lower slopes may create an opposite soil moisture contrast (case S3). Figure 13 illustrates the predicted flow patterns in those cases where, for comparison purposes, the development of flows along homogeneously dry and wet slopes (S1 and S2) are presented in Figure 14. In the case S4 (presented for 1600 LST) a distortion of the typical upslope flow pattern is evident as a counter-circulation between the elevated wet region and the lower dry region is established. The counter-circulation is more apparent when the slope angle is smaller (S4*). The opposite contrast (S3) shows only a slight intensification of the flow at the top of the slope in comparison with the dry slope case (S1).

In order to analyze the dependency of the counter-circulation on the slope angle we will apply Eq. (8) along the path of integration indicated in Fig. 15. The top segment of this path reflects the height of the PBL.

In this section we have

$$\frac{\partial \bar{\pi}}{\partial z^*} < 0, \quad \frac{\partial \theta'}{\partial z^*} < 0 \quad \text{and} \quad \frac{\partial z_G}{\partial x} > 0. \qquad (14)$$

Under these conditions, Eq. (8) indicates:

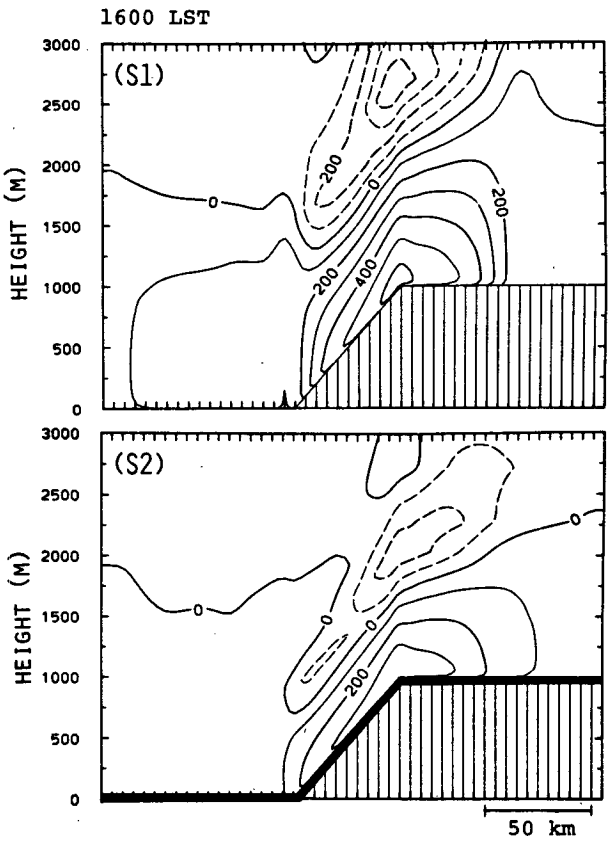

FIG. 14. As in Fig. 8 except for cases S1 and S2.

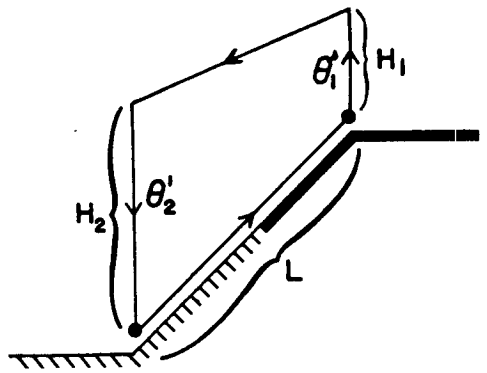

FIG. 15. Schematic illustration of the chosen path of integration for circulation evaluation for the single slope case. The top path reflects the PBL top.

i) If $\partial\theta'/\partial x > 0$ (as with case S3) the circulation (and also the averaged surface flow) intensifies with time ($\partial C/\partial t > 0$).

ii) If $\partial\theta'/\partial x < 0$ (as in cases S4 and S4*) we have

$$\frac{\partial C}{\partial t} > 0 \quad \text{if} \quad \frac{\partial z_G}{\partial x} > \left(\frac{\partial z_G}{\partial x}\right)_{cr}, \qquad (15a)$$

$$\frac{\partial C}{\partial t} < 0 \quad \text{if} \quad \frac{\partial z_G}{\partial x} < \left(\frac{\partial z_G}{\partial x}\right)_{cr}, \qquad (15b)$$

where

$$\left(\frac{\partial z_G}{\partial x}\right)_{cr} = \frac{-\int_S \frac{\partial \theta'}{\partial x}\, dS}{\int_S \frac{\partial \bar{\theta}}{\partial z^*}\, dS} \approx \frac{\frac{1}{L}(\theta_2' - \theta_1')H \cdot L}{\frac{\partial \bar{\theta}}{\partial z^*} H \cdot L} = \frac{(\theta_2' - \theta_1')}{\frac{\partial \bar{\theta}}{\partial z^*}} \cdot \frac{1}{L}, \qquad (16)$$

L is the slope length and $H \approx (H_1 + H_2)/2$.

Let us obtain the critical slope $(\partial z_G/\partial x)_{cr}$ in our situation during the daytime. In our cases (S4) and (S4*), $\partial\bar{\theta}/\partial z^* \approx 4 \times 10^{-3}$ K m^{-1} (based on a rough estimate for the lower 2000 m); $\theta_2' - \theta_1' \approx 3.0$°C at 1600 LST and $L \approx 50$ km. It is worth noting that similar values of $\theta_2' - \theta_1'$ are also obtained in the case of the same moisture contrast over flat terrain (case F4). Substituting these values into (15), we obtain

$$\left(\frac{\partial z_G}{\partial x}\right)_{cr} \approx \frac{1.5}{100}.$$

Hence, for the case (S4) where $\partial z_G/\partial x = 2/100$ according to (15a), $\partial C/\partial t > 0$; namely, the counter flow downward is not dominating. On the other hand, for the case (S4*) where $\partial z_G/\partial x = 1/100$, $\partial C/\partial t < 0$; namely, the downward component dominates the circulation. Similarly, other critical slope angles were approximated for various moisture availability con-

TABLE 2. Critical slope $[(\partial z_G/\partial x)_{cr} \times 100]$ for various contrasts of moisture availability (Δm) at 1600 LST.

Δm				
0.95	0.45	0.25	0.15	0.05
2.0	1.5	1.0	0.7	0.3

trasts (where in the dry section $m = 0.05$); these are given in Table 2 for 1600 LST.

Generally, the analysis results suggest that when the upper portion of a slope is relatively wet as compared to the lower portion (as may occur because of the precipitation distribution), the upslope flow is expected to slow or even to reverse near the zone of the moisture discontinuity. This situation is likely to occur when the magnitude of the soil moisture discontinuity increases, or as the slope steepness is reduced.

4. Conclusion

The current study suggests that thermally induced mesoscale circulations are of sufficient significance to be considered in meteorological evaluations on this scale. It was found that circulations induced by large contrasts in soil moisture along flat terrain can be equivalent in magnitude to that of a sea breeze. Even slight moistening of the ground surface, however, can exert a significant influence on mesoscale flows, and can also alter boundary layer structure.

A very weak synoptic flow was assumed in this study, in order to carry out simple preliminary modeling evaluations, as well as to perform standard scale analysis. When stronger synoptic flow exists, the predicted patterns should be modified. These modifications, however, can be qualitatively evaluated from the knowledge we have about the coupling of the sea breeze with synoptic flows (e.g., Estoque, 1962; Pielke, 1974; Physick, 1976; and Simpson *et al.*, 1977) and the coupling of mountain thermally induced circulations with synoptic flows (e.g., MacHattie, 1968; Skibin and Hod, 1979; and Banta, 1984).

A simple methodology for specification of the soil moisture availability over mesoscale regions is of crucial importance for obervational evaluation of models and for further modeling studies. In recent years, the work of Idso *et al.* (1976), Price (1980), Carlson *et al.* (1981), Grody (1983) and Wetzel *et al.* (1984) suggests procedures to evaluate soil moisture by means of remote sensing using satellites. Utilization of such procedures may indicate areas where mesoscale surface moisture contrasts exist, as well as the involved magnitude of moisture availability contrasts.

Acknowledgments. The current study was supported by Grant No. ATM-8304042 and ATM-8414181 of the Experimental Meteorology and Weather Modification Division of the National Science Foundation, and Grants No. NA 81RA-H-0000, Amend. 12, Item 10 and No. NA81RAH00001, Amend. 17, Item 15 of the National Oceanic and Atmospheric Administration. The senior author was supported by a fellowship from the government of Japan. The model computations were carried out using the NCAR computer; NCAR is supported by the National Science Foundation.

The authors wish to thank Dr. Y. Mahrer for useful discussions and suggestions, to J. L. Song for his comments on the manuscript and to Mrs. S. Rumley for the excellent preparation of the manuscript.

REFERENCES

Anthes, R. A., 1978: The height of the planetary boundary layer and the production of circulation in a sea breeze model. *J. Atmos. Sci.*, **35**, 1237–1239.

Banta, R. M., 1984: Daytime boundary-layer evolution over mountainous terrain. Part I: Observation of the dry circulation. *Mon. Wea. Rev.*, **112**, 340–356.

Benjamin, S. G., 1983: Some effects of differential heating and topography on regional severe storm environment—Numerical simulation of the SESAME IV (9–10 May 1979) case. *Preprints Conf. Numerical Weather Prediction,* Omaha, Amer. Meteor. Soc., 284–290.

Biggs, W. G., and M. E. Graves, 1962: A lake breeze index. *J. Appl. Meteor.*, **1**, 474–480.

Carlson, T. N., and F. E. Boland, 1978: Analysis of urban–rural canopy using a surface heat flux/temperature model. *J. Appl. Meteor.*, **17**, 998–1013.

——, J. N. Dodd, S. G. Benjamin and J. N. Cooper, 1981: Satellite estimation of the surface energy balance, moisture availability and thermal inertia. *J. Appl. Meteor.*, **20**, 67–87.

——, S. G. Benjamin, G. S. Forbes and Y.-F. Lin, 1983: Elevated mixed layers in the regional severe storm environment: Conceptual model and case studies. *Mon. Wea. Rev.*, **111**, 1453–1473.

Clarke, R. H., 1983: Fair weather nocturnal inland wind surges and atmospheric bores: Part I, Nocturnal wind surges. *Aust. Meteor. Mag.*, **31**, 133–145.

Deardorff, J., 1978: Efficient prediction of ground surface temperature and moisture, with inclusion of a layer of vegetation. *J. Geophys. Res.*, **83**, 1889–1903.

De Vries, D. A., 1963: Thermal properties of soils. *Physics of Plant Environment,* W. R. Van Wijk, Ed., Wiley and Sons, 210–235.

Estoque, M. A., 1962: The sea breeze as a function of the prevailing synoptic situation. *J. Atmos. Sci.*, **19**, 244–250.

Grody, N. C., 1983: Severe storm observations using the microwave sounding unit. *J. Climate Appl. Meteor.*, **22**, 609–625.

Idso, S., R. Jackson, B. Kimball and F. Nakayama, 1975: The dependence of bare soil albedo on soil water content. *J. Appl. Meteor.*, **14**, 109–113.

——, —— and R. J. Reginato, 1976: Compensating for environmental variability in the thermal inertia approach to remote sensing of soil moisture. *J. Appl. Meteor.*, **15**, 811–817.

Lanicci, J. M., and T. N. Carlson, 1983: Sensitivity of the planetary boundary layer to changes in soil moisture availability: Some numerical experiments from SESAME IV. *Preprints 13th Conf. Severe Local Storms.* Tulsa, Amer. Meteor. Soc., 328–331.

Lyons, W. A., 1972: The climatology and prediction of the Chicago lake breeze. *J. Appl. Meteor.*, **11**, 1259–1270.

MacHattie, L. B., 1968: Kananaskis Valley winds in summer. *J. Appl. Meteor.*, **7**, 348–352.

Mahrer, Y., and R. A. Pielke, 1977a: A numerical study of the airflow over irregular terrain. *Beitr. Phys. Atmos.*, **50,** 98–113.

——, and ——, 1977b: The effects of topography on sea and land breezes in a two-dimensional numerical model. *Mon. Wea. Rev.*, **105,** 1151–1162.

——, and ——, 1978: The meteorological effect of the change in surface albedo and moisture. *Isr. Meteor. Res. Pap.*, **2,** 55–70.

Manabe, S., 1969: Climate of the ocean circulation. Part I. *Mon. Wea. Rev.*, **97,** 739–774.

McCumber, M. C., 1980: A numerical simulation of the influence of heat and moisture fluxes upon mesoscale circulations. Ph.D. dissertation, University of Virginia, 255 pp.

——, and R. A. Pielke, 1981: Simulation of the effects of surface fluxes of heat and moisture in a mesoscale numerical model. Part I: Soil layer. *J. Geophys. Res.*, **86,** 9929–9938.

McNider, R. T., and R. A. Pielke, 1981: Diurnal boundary layer development over sloping terrain. *J. Atmos. Sci.*, **28,** 2198–2212

Mizzi, A. P., and R. A. Pielke, 1984: A numerical study of the mesoscale atmospheric circulation observed during a coastal upwelling event on 23 August 1972. Part I: Sensitivity studies. *Mon. Wea. Rev.*, **112,** 76–90.

Ookouchi, Y., M. Uryu and R. Sawada, 1978: A numerical study of the effects of a mountain on the land and sea breeze. *J. Meteor. Soc. Japan.* **56,** 368–385.

Philip, J., 1957: Evaporation, and moisture and heat fields in the soil. *J. Meteor.*, **14,** 354–366.

Physick, W. L., 1976: A numerical model study of the sea breeze phenomenon over a lake or gulf. *J. Atmos. Sci.*, **33,** 2107–2135.

——, 1980: Numerical experiments on the inland penetration of the sea breeze. *Quart. J. Roy. Meteor. Soc.*, **106,** 735–746.

Pielke, R. A., 1974: A three-dimensional numerical model of the sea breezes over south Florida. *Mon. Wea. Rev.*, **102,** 115–139.

——, and Y. Mahrer, 1978: Verification analysis of the University of Virginia three-dimensional mesoscale model prediction over south Florida for 1 July 1973. *Mon. Wea. Rev.*, **106,** 1568–1589.

Price, J. C., 1980: The potential of remotely sensed thermal infrared data to infer soil moisture and evaporation. *Water Resour. Res.*, **16,** 787–795.

Sasamori, T., 1970: A numerical study of atmospheric and soil boundary layers. *J. Atmos. Sci.*, **27,** 1122–1137.

Segal, M., and R. A. Pielke, 1981: Numerical model simulation of human biometeorological heat load condition—summer day case study for the Chesapeake Bay area. *J. Appl. Meteor.*, **20,** 735–749.

——, Y. Mahrer and R. A. Pielke, 1982: Application of a numerical mesoscale model for the evaluation of seasonal persistent regional climatological patterns. *J. Appl. Meteor.*, **21,** 1754–1762.

——, —— and ——, 1983: A study of meteorological patterns associated with a lake confined by mountains—the Dead Sea case. *Quart. J. Roy. Meteor. Soc.*, **109,** 549–564.

Simpson, J. E., D. A. Mansfield and J. R. Milford, 1977: Inland penetration of sea-breeze fronts. *Quart. J. Roy. Meteor. Soc.*, **103,** 47–76.

Skibin, D., and A. Hod, 1979: Subjective analysis of mesoscale flow patterns in northern Israel. *J. Appl. Meteor.*, **18,** 329–338.

Sun, W. Y., and Y. Ogura, 1979: Boundary-layer forcing as a possible trigger to a squall-line formation. *J. Atmos. Sci.*, **36,** 235–254.

Walsh, J. E., 1974: Sea breeze theory and application. *J. Atmos. Sci.*, **31,** 2012–2026.

Wetzel, P. J., 1978: A detailed parameterization of the atmospheric boundary layer. Atmos. Sci. Paper No. 302, Dept. of Atmos. Sci., Colorado State University, Fort Collins, 195 pp.

——, D. Atlas and R. H. Woodward, 1984: Determination soil moisture from geosynchronous infrared data: A feasibility study. *J. Climate Appl. Meteor.*, **23,** 375–391.

Zdunkowski, W. G., J. Paegle and J. P. Reilly, 1975: The effect of soil moisture upon the atmospheric and soil temperature near the air–soil interface. *Arch. Meteor. Geophys. Bioklim.* **A24,** 245–268.

Zhang, D. L., and R. A. Anthes, 1982: A high resolution model of the planetary boundary layer-sensitivity tests and comparisons with SESAME-79 data. *J. Appl. Meteor.*, **21,** 1594–1609.